In-situ observation of the phase evolution during an electromagnetic-assisted sintering experiment of an intermetallic γ-TiAl based alloy

Michael Musi, Benjamin Galy, Jean-Philippe Monchoux, Alain Couret, Helmut Clemens, Svea Mayer

In-situ observation of the phase evolution during an electromagnetic-assisted sintering experiment of an intermetallic γ-TiAl based alloy

Michael Musi[a]*, Benjamin Galy[b], Jean-Philippe Monchoux[b], Alain Couret[b], Helmut Clemens[a],
Svea Mayer[a]

[a] Chair of Physical Metallurgy and Metallic Materials, Department of Materials Science, Montanuniversität Leoben, Franz-Josef-Straße 18, 8700 Leoben, Austria

[b] CNRS, CEMES, BP 94347, 29 rue Jeanne Marvig, 31055 Toulouse, France

* Corresponding author: michael.musi@unileoben.ac.at

Abstract: Electromagnetic-assisted sintering offers the possibility for a time-efficient densification of intermetallic γ-TiAl based powders. Since the microstructure of the densified material and, thus, its mechanical properties can be controlled by the imposed temperature profile, the kinetics and transformations of the occurring phases are of particular interest. The present study describes a diffraction setup for the in-situ observation of the phase evolution by high-energy X-ray diffraction during an electromagnetic-assisted sintering process using induction heating. Starting from Ti-46.3Al-2.2W-0.2B powder (in at.%), this experiment grants time-resolved insights into the non-equilibrium and equilibrium phase transformations during this powder consolidation process for the first time. The microstructural accordance of the electromagnetic-assisted sintered specimen with spark plasma sintered material densified at the same dwell temperature highlights the transferability of both techniques and allows an allocation of the determined phase transformation data to the spark plasma sintering technology.

Keywords: Titanium aluminides; Sintering; Phase transformation kinetics; Synchrotron radiation

Intermetallic γ-TiAl based alloys are considered excellent candidates for applications in the automotive and aeronautic industries due to their outstanding material-specific properties. These alloys are characterized by a high creep resistance, a low density of around 4 g/cm^3, depending on the exact alloy composition, and, consequently, excellent specific mechanical properties [1,2]. In the Al range of technical γ-TiAl based alloys, i.e. 42-48 at.%, different phases occur in dependence of the temperature [3]. At low temperatures, the name-giving, ordered tetragonal face-centred γ-TiAl phase and the ordered hexagonal α_2-Ti_3Al phase are stable in binary TiAl alloys. The α_2 phase shows a disorder reaction into the disordered hexagonal α phase upon heating at the eutectoid temperature. Additionally, the disordered body-centered cubic (bcc) β phase occurs at high temperatures in the phase diagram. The alloying with β-stabilizing elements, i.e. Nb, Mo and W, results in its stabilization down to lower temperatures and also higher Al contents as well as in the occurrence of the ordered bcc β_o phase at service temperature [1,3].

Field-assisted sintering includes a variety of different densification techniques distinguishable by the underlying thermal and electrical phenomena [4,5]. Of particular interest for the present work are sintering via an electromagnetic field as well as spark plasma sintering (SPS). While in both cases the material is heated via the Joule's effect, the associated current in the metallic powder is inductively generated in the first case and directly applied in the latter case [5,6]. Furthermore, SPS relies on the additional application of an external pressure. A major advantage of field-assisted sintering techniques based on solid state processes is the possibility of a direct microstructure adjustment [5,7]. By changing the dwell temperature with respect to the alloy's phase diagram, different microstructures and, consequently, tailored mechanical properties can be obtained in γ-TiAl based alloys. Generally, dwell temperatures above the γ-solvus temperature result in a fully lamellar microstructure characterized by excellent creep resistance, but low room temperature ductility. Dwell temperatures situated at lower temperatures within the (α+γ) phase field region result in a so-called near gamma microstructure with a low creep resistance, but superior room temperature ductility [3,8]. Since high heating rates as well as short processing times can be achieved by field-assisted sintering techniques, phase transformation kinetics have a major impact on the occurring phases and, thus, on the final microstructure and the related mechanical properties [3,5]. Therefore, we report here on the use of high-energy X-ray diffraction (HEXRD), a powerful tool for monitoring the phase transformations in γ-TiAl based alloys [9], to investigate for the first time these transformations during an electromagnetic-assisted sintering. Emphasis is laid on the experimental diffraction setup and the resulting phase

evolution, which is discussed regarding the occurring phase transformations. Combined with a microstructural characterization of the in-situ HEXRD specimen and SPS material processed at the same dwell temperature, the present work also highlights the similarities and differences between the described electromagnetic-assisted sintering and the SPS technology.

The alloy investigated in the current study has the composition Ti-46.3Al-2.2W-0.2B (in at.%), which was determined by X-ray fluorescence spectroscopy and inductively coupled plasma atomic emission spectroscopy. The amount of O measured by carrier gas hot extraction is 720 m.-ppm. The powder was produced by electrode induction melting inert gas atomization by GfE Metalle und Materialien GmbH, Germany. Powder in the particle size range of 25-50 µm with a homogeneous microstructure was used for the in-situ HEXRD sintering experiment and the SPS densification, which was conducted on a SYNTEX 2080 machine under vacuum (5-10 Pa) with a temperature of 1325 °C, a dwell time of 120 s, and a pressure of 50 MPa as reported in [8,10]. For the in-situ observation of the phase fractions, the electromagnetic-assisted sintering process has to be implemented in a suitable experimental diffraction setup for the in-situ HEXRD experiment. As the temperature applied to the material is the main driving force for the phase evolution, an exact temperature control is crucial for a successful experiment. This is realized during the sintering process with a modified dilatometer 805A/D by TA Instruments, USA, in which the specimen is heated inductively by an induction coil in a high-purity Ar atmosphere and cooled by Ar gas [11]. A self-designed sample holder served the purpose of containing the powder during the in-situ HEXRD sintering experiment and acting as the attachment point for the thermocouple (type S). A schematic drawing of the sample holder is shown in Fig. 1a. It consists of a hollow tube with a length of 10 mm and an inner radius of 5 mm. Its low wall thickness of 500 µm allows a sufficient penetration of the synchrotron radiation into the material. This hollow tube is sealed by two caps to ensure the containment of the powder during the experiment. The sample holder is made of technical pure Mo to withstand the temperatures during the experiment. Additionally, only a minor contamination of the material is expected due to the low diffusivity of Mo in γ-TiAl based alloys and the short dwelling time. The temperature profile experienced by the material during the in-situ HEXRD sintering experiment matches the temperature profile of a real SPS process and is shown in detail in Fig. 1b [10]. A dwell temperature of 1325 °C and a dwell time of 3 min have been chosen. The in-situ HEXRD sintering experiment has been conducted at the beamline P07 at the storage ring PETRA III at the synchrotron facility Deutsches Elektronen Synchrotron (DESY), Hamburg, Germany, using a synchrotron radiation with a mean photon energy of 73.6 keV. During the experiment,

whole diffraction rings emitted by the material were captured using a Perkin-Elmer X-ray area detector 1621 placed at a distance of approximately 1500 mm behind the specimen (Fig. 1a). The experimental setup was calibrated using a LaB_6 sample. The obtained diffraction data were azimuthally integrated with the software fit2D [12]. The evolution of the volume fraction of the individual phases was determined by sequential Rietveld refinement using the batch processing mode of the software MAUD [13]. Since no phase transformation occurs under the applied cooling rate of 100 °C/min at low temperatures, the experiment was terminated at 700 °C.

The room temperature diffraction spectrum of the powder recorded before starting the in-situ HEXRD sintering experiment, depicted in Fig. 2a, shows several distinct peaks. Along with the peaks of the intermetallic Ti-Al related phases, peaks belonging to the Mo sample holder are also observed (orange diamonds in Fig. 2a). However, these additional Mo peaks need to be accounted for in the Rietveld analysis of the diffraction data by introducing an additional phase. In this material condition, i.e. in the powder, the superstructure peaks belonging to the α_2 phase and the β_o phase could not be detected at room temperature. Generally, these peaks, e.g.
α_2-$(10\bar{1}1)$ and β_o-(100), possess a very low intensity when compared to the main peaks of the respective phases in the HEXRD signal, which is further reduced by the Mo sample holder. So while the presence of the disordered α phase in the powder, as indicated by the absence of the α_2 superstructure peaks, is in accordance with literature, an ordering into α_2 during powder atomization cannot be completely ruled out [14–16]. However, during the in-situ HEXRD sintering experiment, α_2 superstructure peaks were indeed observed. Contrarily, no β_o superstructure peaks occurred in the investigated temperature range. Thus, the present bcc phase will be designated as β/β_o phase, although ordering of this phase during rapid cooling after atomization has been reported in literature [17]. Consequently, it should be mentioned that in the Rietveld analysis the disordered α and β phase have been used to model the hexagonal and the bcc phase throughout the whole experiment.

The evolution of the volume fractions of the α/α_2, the β/β_o and the γ phase during the in-situ HEXRD sintering experiment determined by Rietveld analysis is shown in Fig. 2b. The distribution of the phase fractions at room temperature, i.e. the high amount of α and the rather low amount of γ, is a consequence of the high cooling rate occurring during powder atomization, i.e. 10^5-10^6 °C/s [17], resulting in a material condition far from thermodynamic equilibrium. During the first part of the heating segment, the phase fractions stay relatively

constant due to lack of thermal activation. However, once a temperature of about 700 °C is exceeded, the amount of α drastically decreases, while the amount of γ increases due to the high driving force. Consequently, this non-equilibrium phase transformation shifts the system towards thermodynamic equilibrium. Additionally, the decrease in the α fraction is accompanied by a decrease in the β/β_o fraction. At a temperature of around 920 °C, the metastable α phase undergoes an ordering transformation into the thermodynamically stable α_2 phase as it could be deduced from the occurrence of its superstructure peaks in the diffraction pattern. This α_2 phase disorders again into the α phase upon further heating, i.e. at 1165 °C. The γ phase, which is the alloy's main constituent at this temperature, starts to dissolve and the volume fraction of the disordered α phase strongly increases. Before the dwell temperature of 1325 °C is reached during the experiment, the γ phase has completely dissolved. Thus, only the α and the β/β_o phase, which can be expected to has disordered at this temperature [18], are present during dwelling. Furthermore, an increase of the β/β_o phase fraction is observed after the γ phase dissolution, since the material is moving through the (α+β) phase field region of the alloy system. Consequently, during the cooling segment after dwelling, a lowering of the β/β_o phase fraction is observed. Once the temperature falls below the γ-solvus temperature, a significant amount of γ phase is formed. Further cooling yields the ordering of α into α_2 at around 1120 °C followed by only minor adjustments of the phase fractions. After the in-situ HEXRD sintering experiment, the material consists of 90 vol.% γ, 7 vol.% α_2 and 3 vol.% β/β_o at room temperature as indicated by the respective symbols in Fig. 2b.

In addition to the evolution of the phase fractions, Rietveld analysis of the diffraction data provides insight into the lattice parameters of the occurring phases. Exemplarily, the *c/a* ratio of the α/α_2 phase is shown in Fig. 2c. Prior to the transition towards thermodynamic equilibrium, only a slight decrease of the *c/a* ratio is observable. However, during aforementioned non-equilibrium phase transformation, it increases drastically due to the change in the chemical composition of α. Generally, the *c/a* ratio of the α/α_2 phase is found to increase with increasing Ti content and decreasing Al content [19]. Thus, the Al redistribution between α and γ during this transition towards thermodynamic equilibrium results in the observed *c/a* ratio increase. Furthermore, a discontinuity in the *c/a* ratio occurs during the heating segment (grey area in Fig. 2c). This arises from the momentary presence of two hexagonal phases with different lattice parameters as indicated by the insert in Fig. 2c. This shows the evolution of the hexagonal (200) peak, which, generally, should shift towards lower Bragg angles due to thermal expansion during the heating segment. However, a double peak

rather than an individual peak is observed at 557 s (see arrows). The peak at the higher Bragg angle corresponds to α phase with a composition far from its ideal stoichiometry, while the peak at the lower Bragg angle belongs to a newly formed α_2 phase with an adjusted composition in order to bring the material closer towards thermodynamic equilibrium. Further heating manifests in a decreasing *c/a* ratio due to an Al enrichment, attributed to the fact that the phase boundary separating the (α+β) and the (α+β+γ) phase field region is generally shifted towards higher temperatures with an increasing Al content [17]. Once the γ-solvus temperature is exceeded and the material is within the (α+β) phase field region, the *c/a* ratio remains constant. Its increase during cooling can be attributed to the Al exchange between α and γ in the (α+β+γ) phase field region as well as to the ordering into α_2.

The microstructure of the specimen was investigated by scanning electron microscopy (SEM) to verify the observations of the in-situ HEXRD sintering experiment. For this, the in-situ HEXRD specimen and the as-SPSed material were metallographically prepared as described in [20]. Micrographs of the individual microstructures were taken with a Tescan CLARA SEM, Czech Republic, using backscattered electron (BSE) mode. An overview of the cross-section of the specimen is shown in Fig. 3a. Although no pressure was applied, sintering occurred to some extend during the in-situ HEXRD sintering experiment. However, a high porosity is still present within the material. At the surface of the specimen, a bright layer can be detected in BSE mode indicating a Mo contamination layer. A micrograph of this layer at a higher magnification is depicted in the insert in Fig. 3a. Although, this suggests diffusion of Mo from the sample holder into the material, the thickness of this layer is rather small, i.e. 50 µm, and, thus, is expected to be not significant. The microstructure of the in-situ HEXRD sintering specimen, shown in Fig. 3b, consists of lamellar α_2/γ colonies, which are surrounded by β_o and γ phase. This microstructure is in accordance with the phases observed during the in-situ HEXRD sintering experiment. As described above, α and β phase are present at the dwell temperature, where the β phase limits the α grain growth and, thus, improves the alloy's ductility by reducing the lamellar colony size [7]. During the cooling segment, the α phase transforms into lamellar α_2/γ colonies by the formation of γ lamellae and a subsequent ordering of the remaining α phase into α_2. Additionally, γ phase is formed in the β_o phase, resulting in the formation of a β_o/γ seam around the colony boundaries [7].

Finally, to compare the electromagnetic-assisted sintering experiment with a real SPS process, the microstructure of as-SPSed material of the same alloy, processed at 1325 °C, is shown in Fig. 3c. A comparison with the in-situ HEXRD specimen (Fig. 3b) reveals the same

microstructural features, e.g. the size and shape of α_2/γ colonies as well as the presence of β_o and γ grains at the colony boundaries. The only difference is the absence of pores due to the applied pressure in the case of SPS. This shows that the same microstructure with respect to the phase distribution could be achieved during the described electromagnetic-assisted sintering experiment. As this experiment and the conducted SPS densification share the same temperature profile characteristics as well as essentially the same heating mechanism, i.e. the Joule's effect [6], this ultimately proves that the observed phase evolution can be applied to the SPS cycle. Thus, the insights into the non-equilibrium and equilibrium phase kinetics and transformations generated in this work are transferable to the SPS technology.

This research was funded in part by the Austrian Science Fund (FWF) [Project Number I 3932-N36]. For the purpose of open access, the author has applied a CC BY public copyright licence to any Author Accepted Manuscript version arising from this submission. The support of the DESY management and photon science user office is gratefully acknowledged. We appreciate the commitment of the Helmholtz-Zentrum Hereon beamline staff, who contributed greatly to the success of the experiments performed.

References

[1] S. Mayer, P. Erdely, F.D. Fischer, D. Holec, M. Kastenhuber, T. Klein, H. Clemens, Adv. Eng. Mater. 19 (2017) 1600735.

[2] B.P. Bewlay, S. Nag, A. Suzuki, M.J. Weimer, Mater. High Temp. 33 (2016) 549–559.

[3] H. Clemens, S. Mayer, Adv. Eng. Mater. 15 (2013) 191–215.

[4] S. Asai, Electromagnetic processing of materials, Springer Netherlands, Dordrecht, 2012.

[5] M. Biesuz, T. Saunders, D. Ke, M.J. Reece, C. Hu, S. Grasso, J. Mater. Sci. Technol. 69 (2021) 239–272.

[6] J.R. Keough, J.W.J. Laird, A.D. Godding, ASM-Handbook-4, ASM International, 1991.

[7] T. Voisin, J.-P. Monchoux, M. Perrut, A. Couret, Intermetallics 71 (2016) 88–97.

[8] T. Voisin, J.-P. Monchoux, M. Thomas, C. Deshayes, A. Couret, Metall. Mater. Trans. A 47 (2016) 6097–6108.

[9] P. Spoerk-Erdely, P. Staron, J. Liu, N. Kashaev, A. Stark, K. Hauschildt, E. Maawad, S. Mayer, H. Clemens, Adv. Eng. Mater. (2021) 2000947.

[10] T. Voisin, L. Durand, N. Karnatak, S. Le Gallet, M. Thomas, Y. Le Berre, J.-F. Castagné, A. Couret, J. Mater. Process. Technol. 213 (2013) 269–278.

[11] P. Staron, T. Fischer, T. Lippmann, A. Stark, S. Daneshpour, D. Schnubel, E. Uhlmann, R. Gerstenberger, B. Camin, W. Reimers, E. Eidenberger, H. Clemens, N. Huber, A. Schreyer, Adv. Eng. Mater. 13 (2011) 658–663.

[12] A.P. Hammersley, S.O. Svensson, M. Hanfland, A.N. Fitch, D. Hausermann, High Pressure Res. 14 (1996) 235–248.

[13] L. Lutterotti, Nucl. Instrum. Meth. B 268 (2010) 334–340.

[14] J. Guyon, A. Hazotte, E. Bouzy, J. Alloy. Compd. 656 (2016) 667–675.

[15] D.S. Shih, G.K. Scarr, J.C. Chesnutt, Mater. Res. Soc. Proc. 133 (1988).

[16] D.-Y. Yang, S. Guo, H.-X. Peng, F.-Y. Cao, N. Liu, J.-F. Sun, Intermetallics 61 (2015) 72–79.

[17] M. Kastenhuber, T. Klein, B. Rashkova, I. Weißensteiner, H. Clemens, S. Mayer, Intermetallics 91 (2017) 100–109.

[18] S. Kabra, K. Yan, S. Mayer, T. Schmoelzer, M. Reid, R. Dippenaar, H. Clemens, K.-D. Liss, Int. J. Mat. Res. 102 (2011) 697–702.

[19] L.A. Yeoh, K.-D. Liss, A. Bartels, H. Chladil, M. Avdeev, H. Clemens, R. Gerling, T. Buslaps, Scripta Mater. 57 (2007) 1145–1148.

[20] C. Fleißner-Rieger, T. Pogrielz, D. Obersteiner, T. Pfeifer, H. Clemens, S. Mayer, Pract. Metallogr. 58 (2021) 4–31.

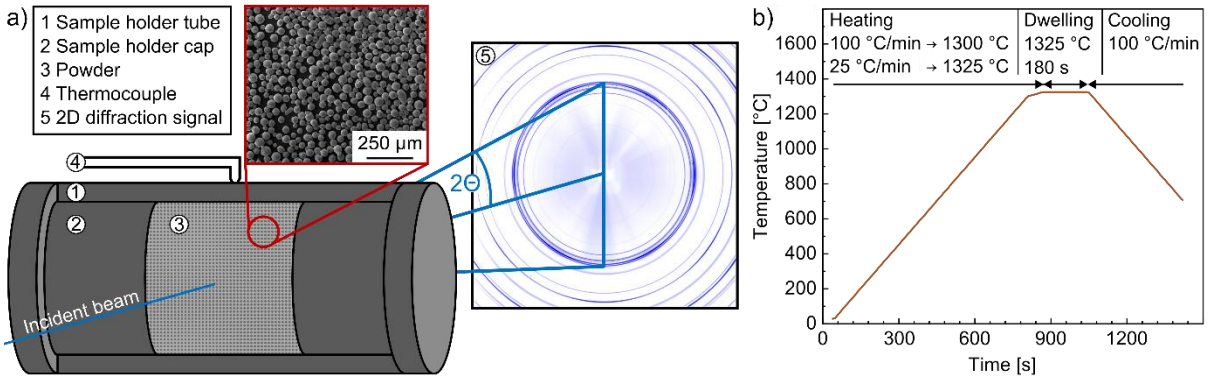

Figure 1. a) Schematic drawing of the experimental diffraction setup. Note that the front side of the Mo sample holder tube is not shown for a better visibility of the material and the sample holder caps; b) temperature profile used for the electromagnetic-assisted sintering during in-situ HEXRD experiment as experienced by the material indicating the heating, dwelling and cooling segment. The sample holder, containing the pre-alloyed powder, is heated inductively via an induction coil in a high-purity Ar atmosphere.

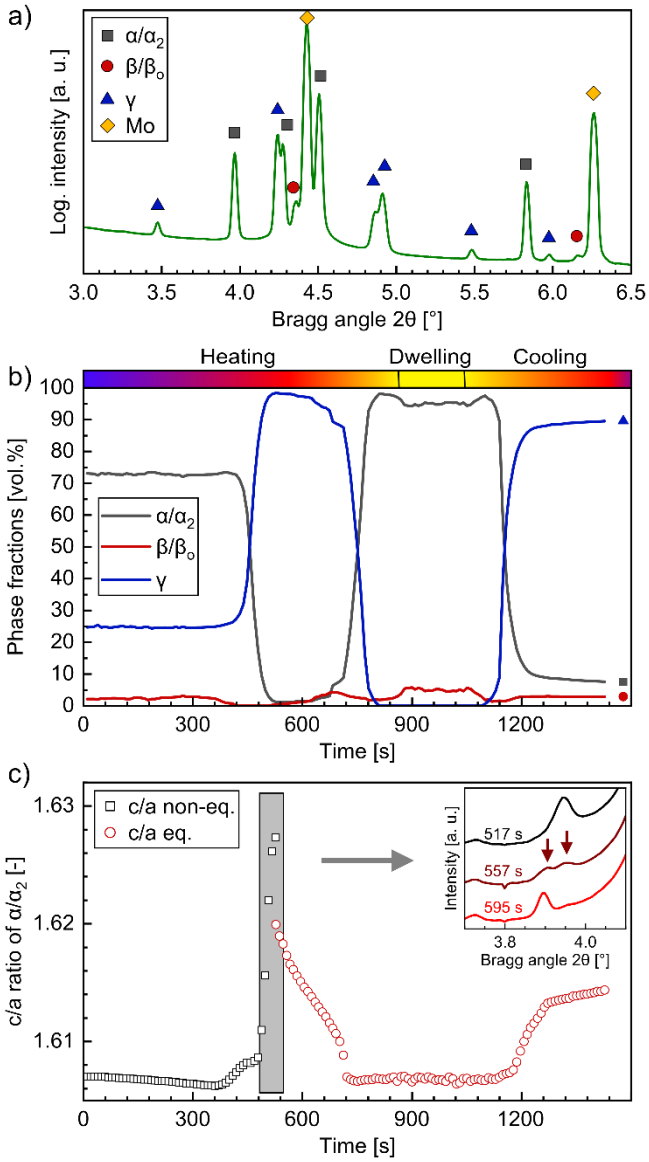

Figure 2. a) Integrated diffraction spectrum of the powder recorded at room temperature before the in-situ HEXRD sintering experiment was started. The peaks belonging to the different phases are marked by individual symbols; b) phase fraction evolution of the α/α_2, the β/β_o and the γ phase in the course of the in-situ HEXRD sintering experiment. The symbols on the right side correspond to the room temperature volume fraction of the α_2 (square), the β/β_o (circle) and the γ phase (triangle); c) evolution of the *c/a* ratio of the α/α_2 phase during the in-situ HEXRD sintering experiment. Note that the presented *c/a* ratio values were extracted from the disordered hexagonal phase model used for the Rietveld analysis. The grey area marks a region, which is characterized by the presence of both hexagonal phases. For a better illustration, the insert presents the diffraction spectra for different times showing the presence of two hexagonal (200) peaks (arrows) at 557 s (for more details see text).

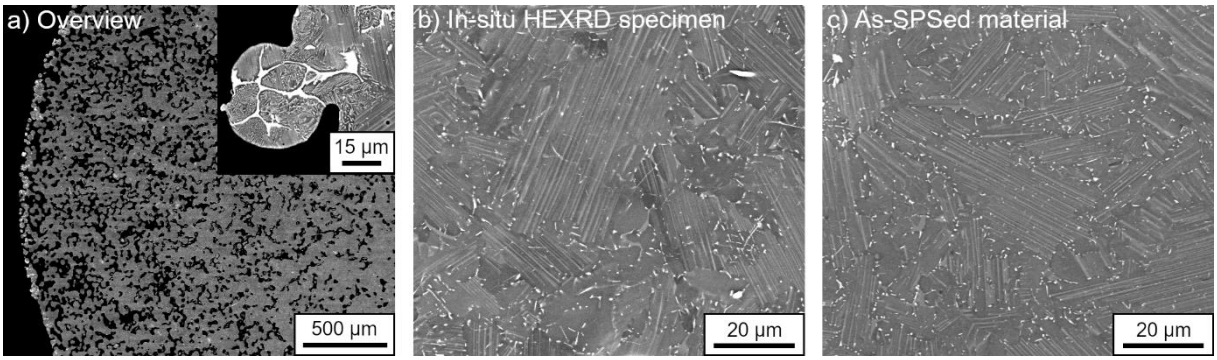

Figure 3. a) Overview of the cross-section of the in-situ HEXRD specimen showing densified areas as well as areas with a high porosity. The insert shows the Mo contamination layer at a higher magnification (see text). In b) and c) SEM-BSE micrographs of the microstructure of the in-situ HEXRD specimen and the as-SPSed material densified at the same dwell temperature are presented. The γ phase exhibits a dark grey contrast, while the α_2 phase appears in a grey contrast and the β/β_o phase shows a bright contrast. No oxides were observed neither in the in-situ HEXRD specimen nor in the as-SPSed material.